

# VELOCITY CORRELATIONS IN DRIVEN TWO-DIMENSIONAL GRANULAR MEDIA

C. BIZON, M. D. SHATTUCK,  
J. B. SWIFT AND HARRY L. SWINNEY  
*Center for Nonlinear Dynamics and Dept. of Physics,  
University of Texas, Austin, TX 78712, USA*

**Abstract.** Simulations of volumetrically forced granular media in two dimensions produce states with nearly homogeneous density. In these states, long-range velocity correlations with a characteristic vortex structure develop; given sufficient time, the correlations fill the entire simulated area. These velocity correlations reduce the rate and violence of collisions, so that pressure is smaller for driven inelastic particles than for undriven elastic particles in the same thermodynamic state. As the simulation box size increases, the effects of velocity correlations on the pressure are enhanced rather than reduced.

## 1. Introduction

In rapid flows of granular media, the mean time between collisions of grains is much longer than the duration of a collision [1]; for such flows, the machinery of kinetic theory is expected to apply. Continuum equations [2, 3] analogous to the Navier-Stokes equations can be produced, allowing quantitative analysis of flows. The simplest and most common formulations incorporate Boltzmann's assumption of molecular chaos: that particle velocities are uncorrelated.

While this assumption works well for low-density molecular gases, granular gases may not abide such a restriction because collisions between grains are inelastic. Inelastic collisions reduce relative velocities, so that post-collisional velocities are more parallel than pre-collisional velocities. Repeated inelastic collisions can lead to strong, long-range velocity correla-

tions, which standard kinetic theory does not include. We will use molecular dynamics simulations to produce steady state granular gases and study the velocity correlations that develop.

The importance and intrinsic interest of velocity correlations in granular flows have been noted by a number of researchers. Two-dimensional simulations of an initially homogeneous distribution of inelastic disks without velocity correlations show that as time progresses, velocity correlations build in both strength and range [4]. These simulations are limited in time, however, because the homogeneous state is unstable to density fluctuations, and rapidly becomes inhomogeneous. Nevertheless, these simulations clearly displayed a characteristic vortex structure of the correlations. Based upon similar considerations, ring kinetic theory, which accounts for velocity correlations, has been applied to the cooling state [5]. One-dimensional simulations of stochastically forced point particles also show velocity correlations [6].

We apply stochastic forcing [6, 7] to two-dimensional event-driven simulations of inelastic disks. The forcing overcomes the tendency of the granular material to form density clusters, and approximately homogeneous steady states form. In an earlier study of these states [8], we found strong velocity correlations that extended throughout the entire simulation area. In the present work, we discuss the simulation method, show that the velocity correlations are essentially independent of the simulated area, and describe the vortex structure of the correlations.

## 2. Simulations of Driven Granular Gases

We treat collisions between molecules as instantaneous and binary. The collisions between grains conserve momentum but dissipate energy. Between collisions, particles travel along straight lines if unaccelerated, or along parabolas if accelerated. This model allows efficient simulation of collections of particles using event-driven molecular dynamics [9, 10].

When particles collide, the component of the relative particle velocity along the line joining particle centers,  $v_n$ , is reversed, and reduced by a factor  $e$ , the coefficient of restitution, which can take values between 1 for elastic particles and 0 for completely inelastic particles. We allow  $e$  to depend on  $v_n$  through

$$e(v_n) = \begin{cases} 1 - Bv_n^\beta & , v_n < v_o \\ \epsilon & , v_n > v_o \end{cases} , \quad (1)$$

where  $B = (1 - \epsilon)(v_o)^{-\beta}$ ,  $\beta = 3/4$  and  $\epsilon$  is a constant, chosen to be 0.7. These parameters give quantitative agreement to experiments on patterns in vertically oscillated granular media [11, 12]. The variation in  $e$  has the ef-

fect of removing inelastic collapse [13], which is a singularity in the inelastic hard sphere model that produces an infinite number of collisions within a finite time [14, 15]. In general, colliding particles also exert frictional forces on one another; for this paper, we assume that the coefficient of friction is zero, so that we are studying only the effects of inelasticity.

Because of inelasticity, the energy of an unforced collection of grains inevitably decreases. To achieve steady states, then, we must force the granular material. Methods that force through boundaries, such as shaking, invariably produce strong inhomogeneities in the system; to achieve near-homogeneity, we force volumetrically, assuming the particles to be in contact with a white-noise heat bath [7]. Whenever two particles collide, the velocities of two other randomly selected particles are changed by amounts  $|\delta\mathbf{v}|\hat{\mathbf{r}}_i$ , where the magnitude of the kicks,  $|\delta\mathbf{v}|$ , are always the same, but the direction vectors,  $\hat{\mathbf{r}}_i$  are randomly chosen for each kicked particle. In addition to the white noise heat bath, we perform a lesser number of runs with two other heat baths. To model the motions of pucks on an air table [16, 17], we can allow particles to accelerate randomly from collision to collision. Finally, we model the effects of a strong heat bath, which we denote the Boltzmann bath, by completely obliterating the velocities of randomly chosen particles, and giving new velocities based on a Boltzmann distribution. The details of all three forcing methods may be found in [8].

We perform simulations of  $N$  disks of diameter  $\sigma$  moving in a two-dimension square of side length  $L$ , which varies from  $52.6\sigma$  to  $420.8\sigma$ . The simulation box is periodic in both directions. The solid fraction, defined as  $N\frac{\pi}{4}\frac{\sigma^2}{L^2}$ , is 0.5 for all runs. Because of the variation of  $e$  with relative normal velocity, the velocity scale  $v_0$  enters; we use  $v_0$  to nondimensionalize velocities, and  $v_0^2$  to nondimensionalize the granular temperature  $T$ . For  $T$  much larger than one, most particle collisions will occur with the high-velocity value of  $e$ , 0.7; for lower  $T$ , a range of  $e$  will occur.

### 3. Dependence of Correlations upon Simulation Area

We denote two particles 1 and 2, and  $\hat{\mathbf{k}}$  the a unit vector pointing from the center of 1 to the center of 2. The velocity of 1 then has a components parallel to,  $v_1^{\parallel}$ , and perpendicular to,  $v_1^{\perp}$ ,  $\hat{\mathbf{k}}$ , as does particle 2. We define two correlation functions

$$\langle v_1^{\parallel}v_2^{\parallel} \rangle = \sum v_1^{\parallel}v_2^{\parallel}/N_r, \quad (2)$$

$$\langle v_1^{\perp}v_2^{\perp} \rangle = \sum v_1^{\perp}v_2^{\perp}/N_r, \quad (3)$$

where the sums are over the  $N_r$  particles such that the distance between the two particles is within  $\delta r$  of  $r$ . For uncorrelated particle velocities,  $\langle v_1^{\parallel}v_2^{\parallel} \rangle$  and  $\langle v_1^{\perp}v_2^{\perp} \rangle$  will both give zero.

In the smallest simulation area,  $L = 52.6\sigma$ , correlations extend the full length of the computational cell. Cell filling structures may be divided into two cases: structures with a natural length that is larger than the box in which they exist and structures that will always grow to fill any finite box. To differentiate between the former and the latter, we performed four simulations with white noise forcing, quadrupling the area at each step, while holding the solid fraction fixed at 0.5. The granular temperature  $T$  is approximately 30, but varies between 28 in the smallest box and 32 in the largest. This variation in temperature is not important; for  $T \gg 1$ , the coefficient of restitution is independent of collision velocity. In this limit, the role of the temperature is simply to set the velocity scale. The velocity correlation functions are shown in Fig. 1. Even in the largest simulation, composed of 112768 particles, the correlations fill the box. However, the correlation functions for the largest simulation are somewhat different from the smaller ones. This is probably due to poorer statistics; in terms of collisions per particle, this run lasted only one-half as long as the next largest.

Because velocity correlations are positive for small separations, particles collide less frequently and with less relative velocity than elastic particles at the same density, for which velocity correlations are much smaller. As a result, less momentum will be transferred through inelastic collisions than through elastic collisions, and the pressure,  $P$ , will decrease.

Assuming that velocity correlations do not exist, the equation of state for dense granular gases is given by [3]

$$P = (4/\pi\sigma^2)\nu T(1 + (1 + e)G(\nu))., \quad (4)$$

The first term on the right hand side,  $(4/\pi\sigma^2)\nu T$ , accounts for momentum transfer due to particle streaming without collisions, while the second term,  $(4/\pi\sigma^2)\nu T(1 + e)G(\nu)$ , accounts for the momentum transfer due to particle collisions [18]. In the absence of velocity correlations,  $G(\nu)$  is defined as  $\nu g(\nu, \sigma)$ , where  $g(\nu, \sigma)$  is the radial distribution function for the particles, evaluated at zero particle separation. Calculation of  $P$  from simulation, via measurement of the virial [19], becomes a measurement of  $G(\nu)$ , which describes the collisional momentum transport. If velocity correlations exist,  $G(\nu)$  will be reduced, since less momentum will be transported collisionally.

Figure 1 shows that the short range velocity correlations depend on the size of the box; therefore,  $G(\nu)$  should also depend on  $L$ . Figure 2 displays  $G(\nu)$  as a function of  $L$  for these four runs. Over about one decade,  $G(\nu)$  scales with  $\log L$ . Clearly this scaling can not continue indefinitely, since unphysical negative values of  $G(\nu)$  would result. Note also, that increasing the box size actually leads to values of  $G(\nu)$  farther from the values for uncorrelated velocities.

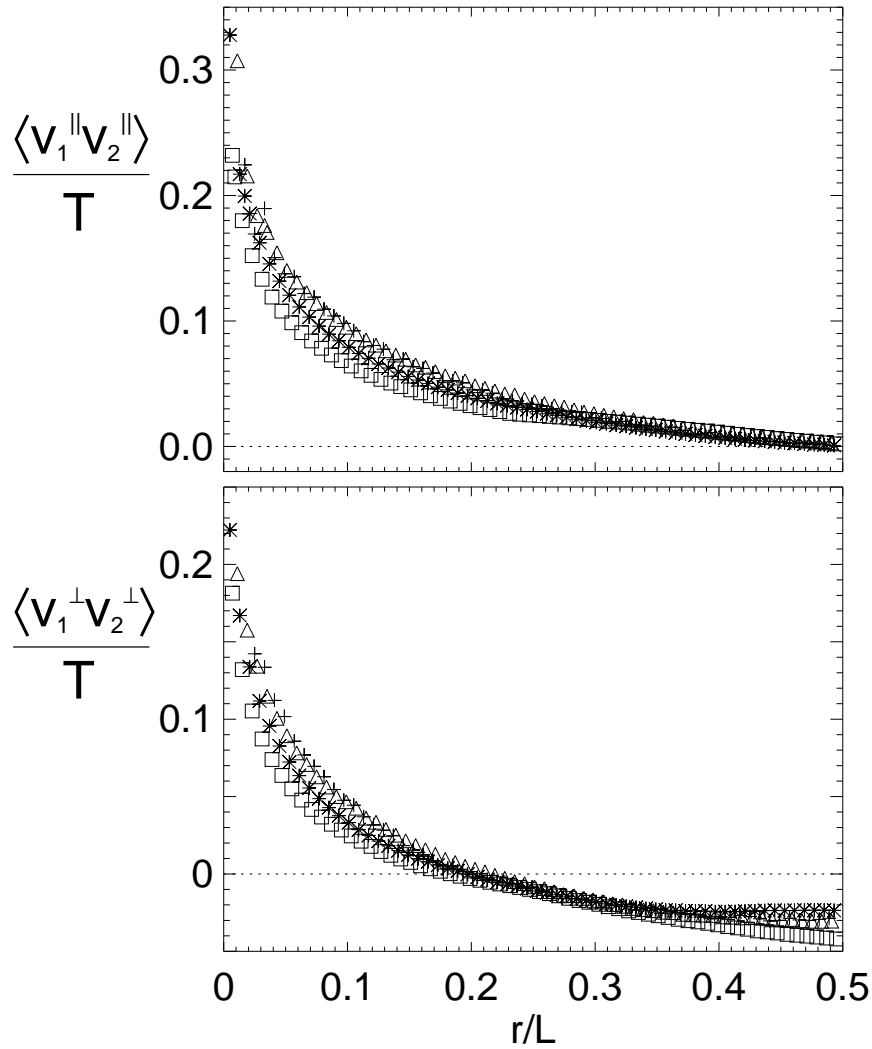


Figure 1. Velocity correlations as a function of particle separation at  $\nu = 0.5$  and  $T \approx 30$ , for four different box sizes. + :  $L = 52\sigma$ ,  $\Delta$  :  $L = 105\sigma$ , \* :  $L = 211\sigma$ ,  $\square$  :  $L = 421\sigma$ .

This unusual result, that the importance of velocity correlations increases with increasing computational area, can also be deduced from the distribution of collision velocities. Figure 3 exhibits these distributions for the runs displayed in Figures 1 and 2. As the computational area increases, so too does the deviation from the distribution predicted for particles chosen without correlation from a Boltzmann distribution, plotted as a solid

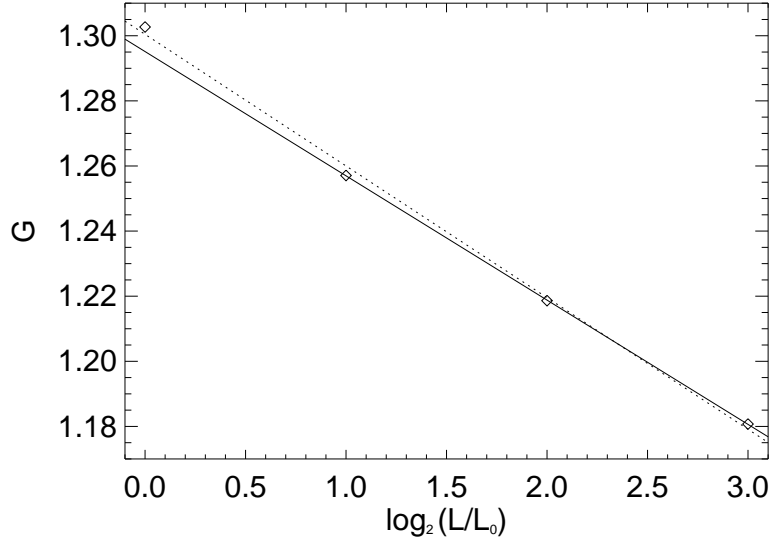


Figure 2.  $G$  as a function of  $L$  for the runs shown in Fig. 1.  $L_o = 52\sigma$  denotes the length of the smallest box. The dotted line is a fit to all four points:  $G(\nu) = 1.3 - 0.04 \log_2(L/L_o)$ . The solid line as a fit to the three largest  $L$  values:  $G(\nu) = 1.295 - 0.038 \log_2(L/L_o)$ . Note that the log is base 2.

curve.

#### 4. Vortex Structure

Inelasticity breeds velocity correlations; reduction of relative velocity in collisions leads to particles moving more alike after collisions than before. On average, then, particles will be surrounded by particles that are moving along with them. The structure of the velocity correlations can be elucidated by calculating this average flow around each particle.

For a single particle  $i$ , we can calculate the flow around it by translating it to the origin, and rotating so that its velocity lies along the positive  $x$  axis. If  $\mathbf{v}(x, y)$  is the velocity field defined by the particles, then the flow around particle  $i$  is given by

$$\mathbf{u}_i = R_{\theta(i)} \mathbf{v}(x - x_i, y - y_i), \quad (5)$$

where  $\theta(i)$  is the angle between the  $i$ -th particle velocity,  $\mathbf{v}_i$ , and the positive  $x$  axis,  $(x_i, y_i)$  is the position of the  $i$ -th particle, and  $R_\theta$  is the operator that rotates vectors clockwise through angle  $\theta$ . The average flow

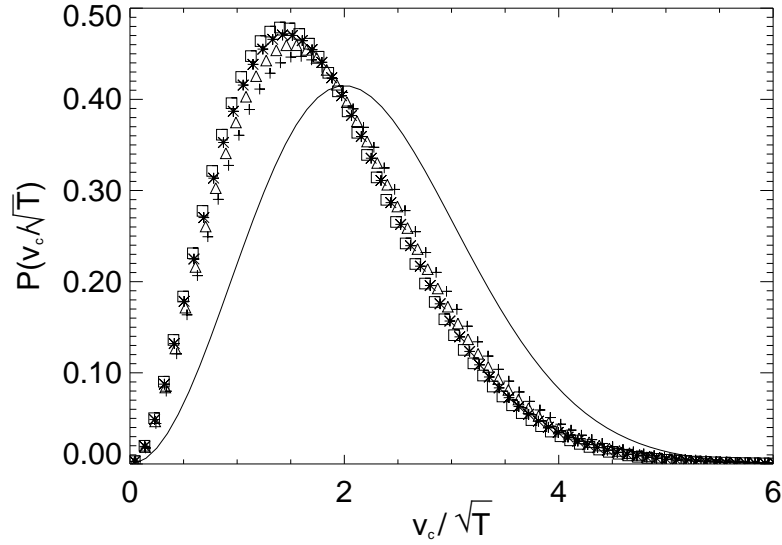


Figure 3. Probability distribution of collision velocities  $v_c = |\mathbf{v}_1 - \mathbf{v}_2|$ , for the data in Figs. 1 and 2. + :  $L = 52\sigma$ ,  $\triangle$  :  $L = 105\sigma$ , \* :  $L = 211\sigma$ ,  $\square$  :  $L = 421\sigma$ . The solid curve is  $P(v_c/\sqrt{T}) = (1/2\sqrt{\pi T^3})v_c^2 e^{-v_c^2/4T}$ , which holds for elastic particles.

around particles, then, is

$$\mathbf{u} = \sum_{i=1}^N \mathbf{u}_i / N. \quad (6)$$

Finally,  $\mathbf{u}$  is averaged over about 100 frames to reduce noise.

Figure 4 displays vector fields of the average flow around particles,  $\mathbf{u}$ , for the three types of forcing, as well as for unforced elastic particles, all at  $\nu = 0.5$  and  $T = 1.05$ . In each case, the vector at the origin, which measures only the average particle speed, has been suppressed, and the longest remaining vector in each field has been scaled to unit length. In both the white noise and accelerated forcings, the average flow near the origin is along the positive  $x$  axis, *i.e.*, with the direction of the central particle's motion. The Boltzmann bath shows some indications of this effect close to the origin, but the correlations are destroyed by the strongly thermalizing forcing before they can propagate to larger length scale. For the elastic particles, there is no discernible flow, only noise.

Close to any particle, surrounding particles move along with it. Farther away, the correlations decay and cannot be seen on Fig 4, so the boxed regions for the white noise forcing and for elastic particles are expanded in Fig. 5. While expansion of the velocity field for elastic particles

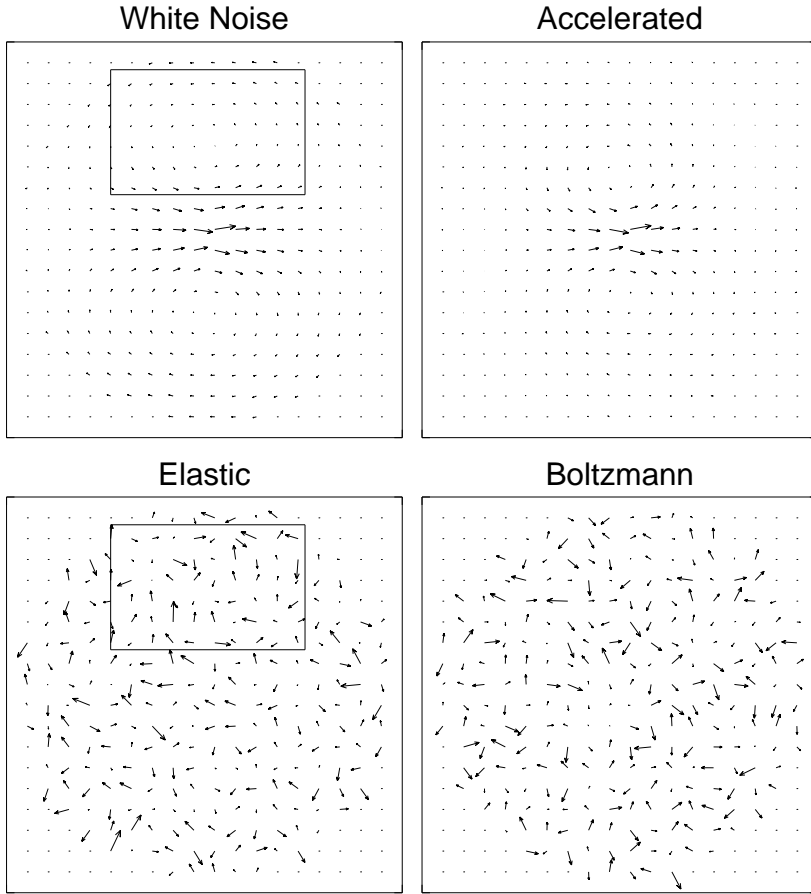
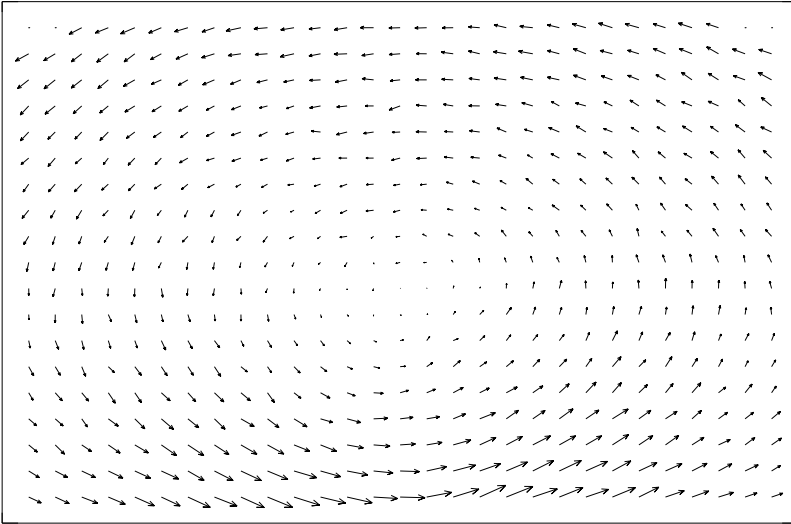


*Figure 4.* The average velocity fields around a particle centered in each cell and moving to the right,  $\mathbf{u}$ , for elastic particles and for inelastic particles forced in three different ways (cf section 2). Each vector field is scaled separately so that its longest vector has length one. Compared to the (suppressed) central vector, these lengths are: White noise, 0.2; Accelerated, 0.27; Boltzmann, 0.008; Elastic 0.008. The boxed regions in the white noise and elastic flows are shown in Fig. 5.

produces still more noise, the inelastic flow field reveals a highly ordered vortex structure. Along the direction of the central particle's motion, the velocities slowly drop to zero, while perpendicular to the original particle's motion, the velocities drop to zero and increase in the negative direction; this flow makes clear the structure of the velocity correlation functions in Fig. 1.

This vortical flow is reminiscent of similar structures produced in simulations of elastic particles [20, 21] by Alder and Wainwright. In their simu-

## White Noise



## Elastic

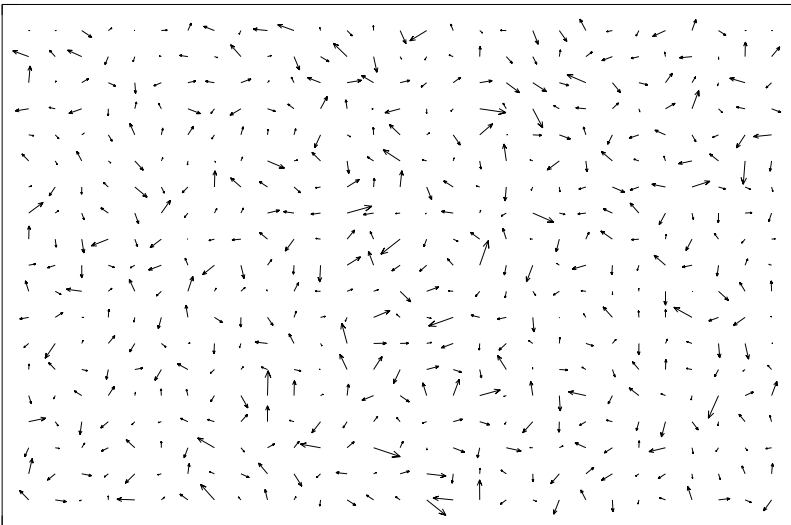


*Figure 5.* A close-up on the boxed regions in Fig 4 reveals that for inelastic particles, large vortices form, one on each side of the particle. The longest vector in the velocity field for inelastic particles represents a velocity nine times larger than that represented by the longest vector for elastic particles.

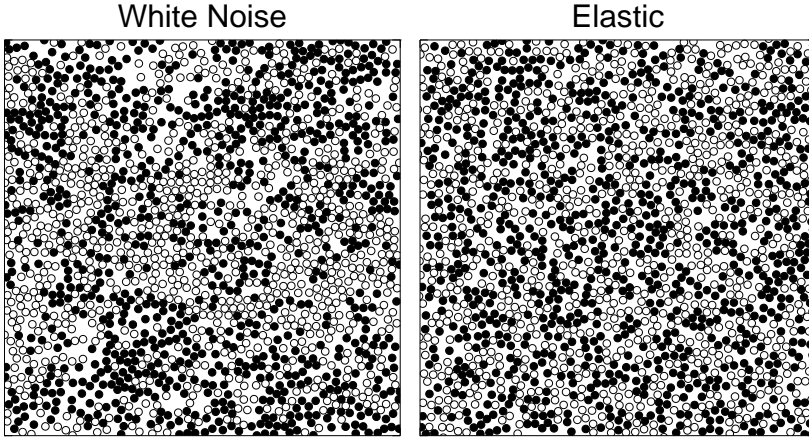


*Figure 6.* Snapshots of simulations with white noise driving and with elastic particles; large coherent structures are visible for the dissipative system on the left. Particles with positive horizontal velocity are black, particles with negative horizontal velocity are white. ( $\nu = 0.5, T = 1.05$ )

lations, they discovered diffusive behavior different from that predicted by kinetic theory. The diffusion constant may be written in terms of the slope of the exponentially decaying autocorrelation function. However, Alder and Wainwright found deviations from exponential decay, and traced the deviations to a vortical flow. If particles  $a$  and  $b$  are initially uncorrelated, an elastic collision will correlate each particle's post collision velocity with the other particle's pre-collision velocity; both particles now have a correlation with the original velocity of particle  $a$ . As particle  $b$  collides with other particles, they gain information about particle  $a$ 's initial velocity. Several collision times later, this information has been transmitted to many particles.

There are two main differences between the vortices in flows of elastic particles and those in flows of inelastic particles. Alder and Wainwright produced the flow field given by

$$\mathbf{u}(t')_i = R_{\theta(i,t)} \mathbf{v}(x - x_i(t), y - y_i(t), t'). \quad (7)$$

For  $t' = t$ , Eq. 5 is recovered; for elastic particles, no structure is apparent. It is only at later times,  $t' > t$ , that a vortex appears in  $\mathbf{u}(t')$ . For the inelastic particles, however, structure is clear at  $t' = t$ . The second difference is the strength of the vortex. The strongest velocity in Alder and Wainwright's vortex was about 2% of the original velocity, while for inelastic particles, the strongest velocity can be about 40% of the central velocity.

The inelastic vortex is so strong that hints of it are visible even in a single snapshot of particles. Figure 6 shows such a snapshot, with particles colored black if they have positive horizontal velocity and white if they have a negative horizontal velocity. For elastic particles, the black and white are well mixed, but in the inelastic case larger scale structure can be glimpsed. Black particles are concentrated along the top and bottom of the image, and white particles are concentrated along the central region.

## 5. Conclusion

The correlations we have found are consistent with those of simulations on the homogeneous cooling state [4]. In those simulations, the range of velocity correlations grew until the onset of large scale density variations. The addition of forcing in our simulations suppresses the growth of density fluctuations, allowing the velocity correlations to continue to grow until they extend throughout the entire computational area.

The results we obtain are not particularly sensitive to the exact form of the forcing. In both the white noise and accelerated forcing schemes, vortical correlation structures form. Only when the bath explicitly destroys correlations, as in the Boltzmann bath, do the results differ.

## 6. Acknowledgments

We thank J. T. Jenkins, M. H. Ernst, and T. P. C. van Noije for useful discussions. This work was supported by the Department of Energy Office of Basic Energy Sciences.

## References

1. C. S. Campbell, *Annu. Rev. Fluid Mech.* **2**, 57 (1990).
2. C. K. K. Lun, S. B. Savage, D. J. Jeffrey, and N. Chepuruiy, *J. Fluid Mech.* **140**, 223 (1983).
3. J. T. Jenkins and M. W. Richman, *Arch. Rat. Mech. Anal.* **87**, 355 (1985).
4. J. A. G. Orza, R. Brito, T. P. C. van Noije, and M. H. Ernst, *Int. J. Mod. Phys. C* **8**, 953 (1998).
5. T. P. C. van Noije, M. H. Ernst, and R. Brito, *Phys. Rev. E* **57**, R4891 (1998).
6. M. R. Swift, M. Boamfä, S. J. Cornell, and A. Maritan, *Phys. Rev. Lett.* **80**, 4410 (1998).
7. D. R. M. Williams and F. C. MacKintosh, *Phys. Rev. E* **54**, R9 (1996).
8. C. Bizon, M. D. Shattuck, J. B. Swift, and H. L. Swinney, Submitted to *Phys. Rev. E* (1999).
9. B. D. Lubachevsky, *J. Comp. Phys.* **94**, 255 (1991).
10. M. Marín, D. Risso, and P. Cordero, *J. Comput. Phys.* **109**, 306 (1993).
11. C. Bizon, M. D. Shattuck, J. B. Swift, W. D. McCormick, and H. L. Swinney, *Phys. Rev. Lett.* **80**, 57 (1998).
12. J. R. de Bruyn, C. Bizon, M. D. Shattuck, D. Goldman, J. B. Swift, and H. L. Swinney, *Phys. Rev. Lett.* **81**, 1421 (1998).

13. D. Goldman, M. D. Shattuck, C. Bizon, W. D. McCormick, J. B. Swift, and H. L. Swinney, *Phys. Rev. E* **57**, 4831 (1998).
14. S. McNamara and W. R. Young, *Phys. Fluids A* **4**, 496 (1992).
15. S. McNamara and W. R. Young, *Phys. Rev. E* **50**, R28 (1994).
16. L. Oger, C. Annic, D. Bideau, R. Dai, and S. B. Savage, *J. Stat. Phys.* **82**, 1047 (1996).
17. I. Ippolito, C. Annic, J. Lemaitre, L. Oger, and D. Bideau, *Phys. Rev. E* **52**, 2072 (1995).
18. S. Chapman and T. G. Cowling, *The Mathematical Theory of Non-uniform Gases* (Cambridge University Press, London, 1970).
19. D. C. Rapaport, *The Art of Molecular Dynamics Simulation* (Cambridge University Press, Cambridge, 1980).
20. B. J. Alder and T. E. Wainwright, *J. Phys. Soc. Japan* **26**, 267 (1968).
21. B. J. Alder and T. E. Wainwright, *Phys. Rev. A* **1**, 18 (1970).